Scaling of impurity fractions for divertor detachment in high-density high-power operation scenarios

A. Huber[1] and A. V. Chankin[2]

[1]Forschungszentrum Jülich GmbH, Institut für Energie- und Klimaforschung – Plasmaphysik, Partner of the Trilateral Euregio Cluster (TEC), D-52425 Jülich, Germany
[2]Max-Planck-Institut für Plasmaphysik, D-85748 Garching, Germany

E-mail: A.Huber@fz-juelich.de

Abstract

For future reactor designs and for planning of operational scenarios in the present and future machines, impurity fractions in the tokamak divertor plasma, c_Z, is an essential input for predictive scalings of divertor detachment. A new quantitative scaling law for c_Z , averaged over the SOL, required to attain detachment is developed for high power H-mode plasmas operated at high densities close to the density limit. It is based on a simple SOL radiation model which uses the combination of the empirical scaling laws for the H-mode power threshold and the separatrix density limit imposed by MHD instabilities. Additionally, it assumes, in agreement with experimental observations that the width of the power conducting layer outside of the separatrix scales approximately with the ion poloidal gyro-radius. The derived expression for c_Z scales strongly with toroidal magnetic field, B, major radius R, the factor of access of the power flow through the separatrix over that required for the L-H transition, f_{LH}, and isotope mass A:

$$c_Z \propto B^{1.47}\, R^{1.59}\, f_{LH}^{1.38} \,/\, A^{1.38}.$$

Estimates of required impurity fractions for divertor detachment for an number of impurity species (N_2, Ne and Ar) in future tokamak reactors ITER and DEMO are made in the paper.

Keywords: detachment, impurities, radiative divertor, tokamaks

1. Introduction

Tokamak operation at high density and high power with a partially or completely detached divertor is considered as the baseline scenario for ITER [1], DEMO [2] and other future fusion

power plants. Divertor detachment enables the conversion of high parallel heat fluxes within the plasma into radiation, preventing localized deposition of heat loads onto divertor targets. The successful reduction of heat loads in the divertor was demonstrated in many present-day machines [3-8]. However, much higher parallel heat fluxes entering the divertor in fusion reactors make it more challenging to dissipate them. Another concern is long term erosion due to physical sputtering by fuel ions and impurities. This requires the electron temperature at the target to be low enough to bring the erosion of the divertor down to acceptable levels. It is also well known that high radiative power losses within the confined plasma can detrimentally affect the plasma energy confinement and fuel dilution, as well as stability of the plasma discharge. It is therefore all the more urgent to understand physical processes in highly radiative discharges to provide the recipe for controlled seeding of impurities with a reasonable reduction in the power flux and target temperature while minimizing the impact on the confined plasma.

High power operation in fusion devices such as ITER and DEMO will require extrinsic impurity seeding to ensure safe operation where stationary surface heat flux densities normal to divertor targets remain at or below 5−10 MWm^{-2} [9,10] to avoid divertor damage. Impurities, such as nitrogen (N_2), neon (Ne) and argon (Ar), are considered as candidate divertor radiators in ITER [11]. Nitrogen and neon proved to be appropriate divertor radiators thanks to their maximum radiative efficiency being at low temperatures, $T_e \sim$ 10-20 eV and $T_e \sim$ 30-50 eV, respectively [12]. On the other hand, the cooling efficiency of Ar reaches peak values at $T_e \sim$ 10-20 eV and $T_e \sim$ 200 eV [12]. Ar is also considered as an important applicant for simultaneous increase of core and divertor radiation, when a certain amount of radiation in the main chamber is requested.

Impurity concentrations necessary to exhaust power to enable detachment is of central importance for future fusion devices, including ITER and DEMO. Knowledge of the impurity concentrations is necessary in order to design and operate future fusion power plants in such a way that the heat and particle flows to the material surfaces are safely limited. In addition, understanding the c_Z is important in assessing fuel dilution and the effects of impurities on key plasma parameters, including parameters that determine the pedestal, and therefore core performance. Recently, several scalings for the impurity fraction required to attain detachment have been developed. They predict the impurity fraction c_Z, defined as the ratio of impurity to electron density, for different plasma parameters [13-15]. These scalings assumed that c_Z is constant along the magnetic field in the SOL and therefore represents the averaged value of the impurity fraction in the scrape-off layer. It should be noted, however, that for conductive

parallel heat flow the plasma radiation in the scrape-off layer will peak in the region of the largest parallel temperature gradients which are expected to be close to the divertor and around the X-point [16,17]. Consequently, the variations of c_Z along field lines are also expected. In our analysis variations in T_e and n_e along field lines in the SOL are taken into account. Similar to [14,15], the proportionality between SOL and divertor c_Z is assumed in order to be able to examine the dependence of c_Z on the average ion mass. To get an insight into variations of c_Z along field lines dedicated experiments in JET and subsequent EDGE2D-EIRENE runs are planned.

In [13] the recipe is presented to predict the seed impurity fraction required to achieve partial detachment for a given P_{SOL} (power flowing through the last closed magnetic flux surface to the scrape-off layer) in devices with a closed divertor similar to that of ASDEX Upgrade (AUG). One of the main results of this study was the dependence of c_Z on the neutral pressure in the divertor, which is not taken into account in the other two studies [14, 15]. Goldston et al. [14] predict the impurity fraction in terms of scrape-off layer (SOL) plasma parameters such as upstream density, separatrix power flow and poloidal magnetic field, with no explicit size scaling. Their scaling assumes that the width of the power conducting layer outside the separatrix scales with poloidal gyro-radius, ρ_p, [18,19] and correspondingly it has a clear isotope dependency due to $\rho_p \sim A^{0.5}$. In [15], empirical scalings for the heat flux width and the H-mode power threshold, P_{LH}, are used alongside a simple SOL radiation model to estimate required impurity fractions. These scalings yield the $B^{0.88}R^{1.33}$ dependence for a given density at the separatrix (or the Greenwald fraction, f_{GW}). No isotope mass or effective charge Z_{eff} dependencies are considered in this approach.

A profitable thermonuclear reactor should operate at maximal possible plasma density to maximise the fusion power which scales quadratically with density [20]. However, the density at the separatrix is limited due to MHD instability in the SOL close to the separatrix, $n_{e,sep} < n_{e,sep}^{crit}$, as shown in [21]. Note that the critical separatrix density $n_{e,sep}^{crit}$ has a strong dependence on the isotopic mass: it is up to 35% lower in the hydrogen (protium) than in the deuterium plasma [22]. Additionally, the critical density depends on the 'effective charge' Z_{eff} and 'average charge' $\bar{Z}$. By reaching the critical separatrix density $n_{e,sep} = n_{e,sep}^{crit}$, ballooning instability triggers SOL turbulence which is spreading into the transport barrier and, by coupling of the transport between core and SOL throughout the pedestal [23] resulting in the back H-L transition. Therefore future fusion devices will have to operate at or close to this limit, so one

can assume $n_{e,sep} = f_{ne}\, n_{e,sep}^{crit}$ with f_{ne} <1. It is therefore important to predict c_Z in terms of operation parameters including the isotope dependence (average mass $\bar{A}$), the 'effective charge' Z_{eff} and 'average charge' $\bar{Z}$, as well as $n_{e,sep}^{crit}$ based on the MHD instability analysis. This work concentrates on the development of the scaling for impurity fractions necessary to exhaust power in the SOL and divertor enabling plasma detachment from divertor targets in high power and high density plasma which will fulfil the above mentioned requirements. The proposed scaling is based on a simple SOL radiation model by using empirical scalings for the power scrape-off width, H-mode power threshold and the scaling for $n_{e,sep}^{crit}$.

The outline of the present paper is as follows. Section 2 briefly describes a simple model for the power exhaust in the SOL. Section 3 introduces a 1D model for impurity radiation. In section 4 an empirical scaling for impurity fraction c_Z required to prompt the pronounced detachment in the divertor is developed using the combination of empirical scaling laws for the SOL heat flux width, H-mode power threshold and the critical density $n_{e,sep}^{crit}$. In section 5 we discuss projections of the obtained scaling onto future tokamak reactors ITER and DEMO. A summary of the work is given in section 6.

2. Power flux balance in the SOL

A model for the power exhaust in the SOL is based on the equality between the power flow across the plasma boundary, which may be the magnetic separatrix or, more generally, last closed flux surface (LCFS) , P_{SOL}, and parallel (to the magnetic field) power flow to divertor targets. An exponential radial decay of the parallel power flow is assumed. Since the power flow across the LCFS is known to be mostly conductive, it can be represented in the diffusive form as:

$$P_{SOL} = q_\perp S \approx -n\chi_\perp \nabla_\perp T\, S \qquad (1)$$

where $q_\perp$ is the perpendicular (across magnetic surfaces) power flux, $\chi_\perp$ is perpendicular thermal diffusivity, and S is the area of the LCFS:

$$S = 4\pi^2 Ra\sqrt{(1+\kappa^2)/2} \qquad (2)$$

where $\kappa = b/a$ is plasma elongation, with a being horizontal minor radius and b the height of the plasma measured from the equatorial plane. In Eq. (1) n is electron density and $T \equiv T_e$ is electron temperature.

The power flowing through the SOL to the divertor along magnetic field lines typically (in the conduction limited regime) is also diffusive and can be expressed as:

$$q_{||}S_{||} = K_{||}\nabla_{||}TS_{||} \approx -n\chi_{||}\nabla_{||}TS_{||} \quad (3)$$

where $q_{||}$ is parallel power flux, $\chi_{||}$ and $K_{||} = n\chi_{||}$ are parallel thermal diffusivity and conductivity, $S_{||}$ is the SOL cross-sectional area perpendicular to magnetic field $\vec{B}$, given by:

$$S_{||} \approx 2\pi R\lambda_q \sin\gamma \approx 2\pi R\lambda_q B_\theta/B$$

where γ is the field line angle at the outboard mid-plane, B_θ and B are poloidal and total magnetic field strengths, and λ_q is the (exponential) perpendicular decay length of the power flux.

Approximating $\nabla_\perp T \approx -T/\lambda_T$, where λ_T is the electron temperature perpendicular decay length in the SOL, perpendicular (from the plasma core into the SOL) and parallel (along SOL flux tubes to the divertor target) power flows to be balanced ($P_{SOL} = Sq_\perp = S_{||}q_{||}$) can be expressed by the following equations:

$$q_{||} = n\chi_{||}\nabla_{||}T = \frac{B}{B_\Theta}\frac{P_{SOL}}{4\pi R\,\lambda_q} \quad (4)$$

$$q_\perp = n\chi_\perp\frac{T}{\lambda_T} = \frac{P_{SOL}}{4\pi^2 Ra\,((1+\kappa^2)/2)^{1/2}}\ . \quad (5)$$

The factor $4\pi R\lambda_q$ in the denominator of Eq. (4), instead of $2\pi R\lambda_q$, reflects an assumption that the power crossing the SOL goes to both inner and outer divertors.

For parameters typically used in recent JET seeding experiments: B=2.5 T, B_θ=0.39 T, P_{SOL}=14 MW, R=2.9 m and λ_q=2.5 mm we calculate $q_{||} = 985\ MW\ m^{-2}$.

3. Simple 1D model for impurity radiation

In the conduction-limited regime the plasma power flux parallel to the magnetic field can be written as [24,25]:

$$q_{||} = \frac{P_{SOL}}{S_{||}} = -k_{0e}{T_e}^{5/2}\nabla_{||}T_e \quad (6)$$

where the electron thermal conductivity constant, k_{0e}, has a value of ≈ 2046 (for ions $k_{0i} \approx 59$) in the plasma with ion species of charge $Z_i = 1$ and T_e in eV. The electron heat conduction is typically the dominant channel for power flux to the target.

For ion species with $Z_i \neq 1$, the electron thermal conductivity constant should be corrected [25]:

$$k_{0,e} = 2046 \cdot G_Z(Z_i) \left[\frac{W}{m\, eV^{\frac{7}{2}}}\right] \tag{7}$$

where G_Z is the correction factor which was discussed in Ref. [26] (in that paper it was denoted as $f^{app}(Z_i)$ instead of G_Z).

The function G_Z is given by:

$$G_Z(Z_i) = \frac{4.295}{Z_i} \left(\frac{Z_i+0.21}{Z_i+4.2}\right). \tag{8}$$

A similar expression $f^{HD}(Z_i) = \left(\frac{5}{Z_i+4}\right)$ was used in [19], which is larger by factors 1.001, 1.089, 1.119, 1.134 and 1.164 than $G_Z(Z_i)$ for Z_i=1,2,3,4 and ∞, respectively. For a multi-component plasma in [26] it was proposed to use Z_{eff} instead of some simple average of individual ion states with charge Z_i.

Since we will later use the expression for the SOL power width predicted by the heuristic particle drift-based model [19] which uses the ratio $\left(\frac{5}{Z_{eff}+4}\right)$, we are adopting here the correction function $G_Z = \left(\frac{5}{Z_{eff}+4}\right)$. The expression for the electron thermal conductivity constant then becomes:

$$k_{0,e} = 2046 \left(\frac{5}{Z_{eff}+4}\right) \left[\frac{W}{m\, eV^{\frac{7}{2}}}\right] = k_0\, G_Z \left[\frac{W}{m\, eV^{\frac{7}{2}}}\right] \tag{9}$$

where $k_0 = 2046$ is the electron thermal conductivity constant at Z_{eff}=1 given in $W\, m^{-1}\, eV^{-7/2}$.

The heat flux $q_{||}$ is reduced by impurity radiation as well as by hydrogenic ionization radiation R_H,

$$\frac{dq_{||}}{dl} = n_e n_Z L_Z(T_e) + R_H \tag{10}$$

where l is the distance along the field line, $n_Z = n_e c_Z$ is impurity density, $c_Z = n_Z/n_e$ is the impurity density fraction, $L_Z(T_e)$ is the cooling rate coefficient due to impurities, which depends only on electron temperature assuming coronal equilibrium. In the coronal equilibrium, when transport processes are slow enough, ionisation stages of impurities are in the equilibrium determined by electron temperature. This typically occurs in the plasma core. At the same time, in the plasma edge and in the divertor region the impurity residence time may be shorter than time scales of ionisation and recombination. Consequently the local equilibrium cannot be assumed for the calculation of radiative power losses. We will come back for the detailed discussion of this issue in section 4. We assume, in agreement with experimental data, that the volumetric power loss (the right hand side (RHS) of Eq. 10) is dominated by impurity radiation and neglect R_H.

In this paper, we will use the technique known as the Lengyel model [27] for deriving an equation relating the drop in the parallel power flux with the radiated power, which was also used in Refs. [14,15]. The Lengyel model assumes that the main energy loss mechanism is radiation loss, neglecting other energy loss mechanisms such as neutral losses, radial transport, and convective energy losses near the target. Therefore, the model may overestimate the c_Z required for divertor detachment. By multiplying Eqs. (6) and (10) and integrating the product $q_\parallel \frac{dq_\parallel}{dl} = \frac{1}{2}\frac{dq_\parallel{}^2}{dl}$ along the magnetic field line from the target (t) to the upstream (u), we obtain:

$$q_{\parallel,u}^2 - q_{\parallel,t}^2 = 2\ p_{e,u}^2 k_{0,e} c_Z \int_{T_{e,t}}^{T_{e,u}} L_Z\,(T'_e)\sqrt{T'_e}\,dT'_e. \tag{11}$$

Here c_Z is assumed to be constant along the magnetic field, and parallel pressure balance is used,

$$p_{e,u} = n_e T_e = n_{e,u} T_{e,u}. \tag{12}$$

Using the standard two point model approach of assuming $T_{e,u} \gg T_{e,t}$ and $q_{\parallel,u} \gg q_{\parallel,t}$ during the advanced detached divertor state, the left hand side (LHS) of Eq. (11) can be simplified:

$$(q_{\parallel,u}^2 - q_{\parallel,t}^2) = \left(q_{\parallel,u} - q_{\parallel,t}\right)\left(q_{\parallel,u} + q_{\parallel,t}\right) \approx (q_{\parallel,u} - q_{\parallel,t})\, q_{\parallel,u} = f_{rad,SOL}\, q_{\parallel,u}^2. \tag{13}$$

Here it is assumed that the radiation fraction $f_{rad,SOL}$ is equal to the fraction of $q_{\|}$ which is removed by radiation, $(q_{\|,u} - q_{\|,t}) \,/\, q_{\|,u}$.

Substituting this into Eq. (11) we obtain:

$$f_{rad,SOL} = \frac{2\, p_{e,u}^2\, k_{0,e} c_Z}{q_{\|,u}^2} \int_{T_{e,t}}^{T_{e,u}} L_Z\,(T'_e)\sqrt{T'_e}\, dT'_e = \frac{2 p_{e,u} k_{0,e} c_Z}{q_{\|,u}^2}\; L_{INT} \tag{14}$$

where we defined $L_{INT} = \int_{T_{e,t}}^{T_{e,u}} L_Z\,(T'_e)\sqrt{T'_e}\, dT'_e$.

A scaling for impurity fraction c_Z for the advanced detached divertor state can be derived from Eq. (14) by assuming that $f_{rad,SOL}$=1:

$$c_Z = \frac{q_{\|,u}^2}{2\, n_{e,u}^2 T_{e,u}^2\, k_{0,e}\, L_{INT}}\,. \tag{15}$$

The upstream separatrix temperature, $T_{e,u}$=$T_{e,sep}$, may be evaluated using the two point model of the SOL transport [28]:

$$T_{e,u} \approx \left(\frac{7\, q_{\|,u}\, L_{\|}}{2 k_{0,e}}\right)^{2/7} \tag{16}$$

where $L_{||}$ is the upstream to target connection length.

Substituting the upstream temperature, $T_{e,u}$, into Eq. (15), one obtains:

$$c_Z = \frac{q_{\|,u}^{10/7}}{4.09\;\; {k_{0,e}}^{3/7}\, n_{e,u}^2\, L_{INT}\, L_{\|}^{4/7}} = \frac{q_{\|,u}^{10/7}}{4.1\;\; {k_0}^{3/7}\, G_Z^{3/7}\, n_{e,u}^2\, L_{INT}\, L_{\|}^{4/7}}\,. \tag{17}$$

The dependence on the upstream separatrix density $n_{e,sep}$=$n_{e,u}$ can be eliminated by using the definition of the Greenwald fraction for the separatrix density, $f_{GW,sep} = 10^{-14}\, n_{e,sep}/(\frac{I_p}{\pi a^2})$, where a is minor radius and I_p is plasma current, both given in SI units: A and m^{-3}. The plasma current dependence in turn can be eliminated by using the cylindrical approximation for the safety factor:

$$q_c = \left(2\pi a^2 B\right)/(R I_p\, \mu_0)(1 + \kappa^2)/2 \tag{18}$$

where $\mu_0 = 4\pi \cdot 10^{-7} H/m$ is magnetic permeability. Thus, the upstream separatrix density can be expressed by:

$$n_{e,u} = 10^{14}\, f_{GW,sep}\, \frac{B\,(1+k^2)}{q_c\,\mu_0\,R} \quad \text{or} \tag{19}$$

$$n_{e,u} = f_{ne}\, n_{e,u}^{crit} = 10^{14} f_{ne}\, f_{GW,sep}^{DL}\, \frac{B\,(1+k^2)}{q_c\,\mu_0\,R} \tag{20}$$

where $f_{GW,sep}^{DL}$ is the density limit caused by an MHD instability in the SOL close to the separatrix. The expression for $f_{GW,sep}^{DL}$ will be given below in section 4.

Combining Eqs. (17) and (20) to eliminate $n_{e,u}$ and taking $L_{\|} = l_{\|}^{*}\ \pi q R$, corresponding to the case of the poloidally constant flux density across the separatrix, we arrive at:

$$c_Z = 7.65 \times 10^{-43}\, \frac{q_{\|,u}^{10/7} q_c^{10/7} R^{10/7}}{\left(f_{ne}\, f_{GW,sep}^{DL}\right)^2\ B^2\ (1+k^2)^2\ \ L_{INT}\, l_{\|}^{*4/7}}\, \frac{1}{G_Z^{3/7}} \tag{21}$$

where we introduced the dimensionless factor $l_{\|}^{*}$ to account for a possibility of extended field lines in some alternative configurations. The heat flux $q_{||}$ here is given in units W/m^2, B in T and L_{INT} in Wm^{-3} eV$^{3/2}$. Note that similar results to Eqs. (15) and (21) were obtained in the previous study in [15] (Eqs. 8 and 9), which is expected since the same Lengyel model was used in this work as in [15].

Substituting $q_{\|}$ (Eq. 4) into Eq. (21) we obtain for the impurity fraction:

$$c_Z = 2.06 \times 10^{-44}\, \frac{P_{SOL}^{10/7}}{\lambda_q^{10/7}}\, \frac{B^{-4/7}}{B_\theta^{10/7}}\, \frac{q_c^{10/7}}{\left(f_{ne}\, f_{GW,sep}^{DL}\right)^2\ (1+k^2)^2\ \ L_{INT}\, l_{\|}^{*4/7}}\, \frac{1}{G_Z^{3/7}}\,. \tag{22}$$

4. Analytical scaling for impurity fractions at the onset of detachment in high density H-mode seeded plasmas

Tokamak operation at high density with a semi-detached or completely detached divertor is considered as the baseline scenario for ITER [1] and DEMO [2] as well as for other future fusion power plants. Because fusion power scales quadratically with n_e, the density limit also restricts the fusion power attainable for a given plasma current I_p. Therefore the establishment

of a detached divertor at densities close to the Greenwald limit, n_{GW}, is unavoidable for maximising the fusion power.

Goldston et al. [21] have recently developed a model for the density limit based on the heuristic drift-based model for the power scrape-off width. It assumes that the H-Mode density limit is caused by an MHD instability in the SOL close to the separatrix and that the SOL total plasma beta (β, the ratio of plasma pressure to magnetic pressure) limit is characterized by the MHD ballooning parameter α as $\alpha_{crit} \approx C_\alpha(1+\kappa^2)^\gamma$. Goldston et al. introduced a factor C_α, which includes the dependence of the ballooning parameter on the magnetic shear s. The derived density limit fraction is given by:

$$f_{GW}^{DL} = 8.13\, C_\alpha \frac{\bar{n}}{n_{sep}} \left(\frac{q_c\, RB}{a} P_{SOL}\right)^{-1/8} (1+\kappa^2)^{\gamma-3/2} \left[\frac{2\bar{A}}{(1+\bar{Z})}\right]^{9/16} \left(\frac{Z_{eff}+4}{5}\right)^{-1/8} \tag{23}$$

where $\bar{n}\ and\ n_{sep}$ are the line-averaged and separatrix densities, Z_{eff} and $\bar{Z}$ are the 'effective charge' and 'average charge' of all ions. In our case the above density limit fraction is normalized to the separatrix density rather than to the line-averaged density, hence we are removing the ratio $\bar{n}/n_{sep}$ from this equation:

$$f_{GW,sep}^{DL} = 4.85\, C_\alpha \left(\frac{q_c\, RB}{a} P_{SOL} l_\parallel^*\right)^{-1/8} (1+\kappa^2)^{\gamma-3/2} \left[\frac{2\bar{A}}{(1+\bar{Z})}\right]^{9/16} \left(\frac{Z_{eff}+4}{5}\right)^{-1/8}. \tag{24}$$

The density limit scaling Eq. (23) was derived for $l_\parallel^* = 1$ and using a different definition for the connection length, $L_\parallel = \pi/2 \cdot q_c R$, in [21]. In addition, an error in the expression of $T_{e,u}$ from the two-point model was discovered in [21]: mistakenly an additional term of π was used in the denominator of T_e. The scaling is updated here by including the dependence on $l_\parallel^*$, by correction of the $T_{e,u}$ term and by using the current definition of the connection length $L_\parallel = l_\parallel^* \pi q_c R$ (see Appendix A), resulting in the appearance of new factor 4.85 in Eq. (24). The derived $f_{GW,sep}^{DL}$ scaling, Eq. (24), shows little variation with key plasma parameters. At the same time, it shows a relatively strong dependence on the average atomic mass of plasma ion species $\bar{A}$. It has to be noted that Greenwald fractions observed in JET-ILW experiments in deuterium and hydrogen plasmas are consistent with the Goldston's prediction [22].

A stability limit $\alpha_{crit} \approx 0.4s(1+\kappa^2)$ was proposed in [29] for elliptical plasmas with elongation κ and magnetic shear $s = d\ ln\ q/d\ ln\ r$ (typically *s*=2). This formula for the ballooning stability parameter was used in some previous publications, e.g. in [30], for the evaluation of the scaling of the Greenwald density limit in the H–mode. The $\alpha_{crit} \approx C_\alpha(1+\kappa^2)^\gamma$ formula used by Goldston matches the expression given in [29] when $C_\alpha \approx 0.4s$ and $\gamma = 1$ are assumed. Following Ref. [30] we will use this assumption in our derivations. Taking *s*=2 for the magnetic shear gives:

$$f_{GW,sep}^{DL} = 3.88 \left(\frac{q_c R B}{a} P_{SOL} l_\parallel^*\right)^{-\frac{1}{8}} \frac{F_{AZ}}{\sqrt{(1+\kappa^2)}} \tag{25}$$

where F_{AZ} is defined as:

$$F_{AZ} = \left[\frac{2\bar{A}}{(1+\bar{Z})}\right]^{9/16} \left(\frac{5}{Z_{eff}+4}\right)^{1/8} = 2^{9/16}\ G_A^{9/16}\ G_Z^{1/8} \tag{26}$$

with $G_A = \frac{\bar{A}}{1+\bar{Z}}$ and $G_Z = \frac{5}{Z_{eff}+4}$.

Substituting $f_{GW,sep}^{DL}$ from Eq. (25) into Eq. (22) gives the following expression for c_Z:

$$c_Z = 1.37 \times 10^{-45} \frac{P_{SOL}^{\frac{47}{28}}}{\lambda_q^{\frac{10}{7}}} \frac{B^{-\frac{9}{28}}}{B_\theta^{\frac{10}{7}}} \frac{1}{{f_{ne}}^2} \frac{q_c^{\frac{47}{28}}}{(1+k^2)\ L_{INT}\ l_\parallel^{*\frac{9}{28}}} \frac{\epsilon^{-1/4}}{{F_{AZ}}^2} \frac{1}{G_Z^{3/7}} \tag{27}$$

where ϵ is the inverse aspect ratio *a/R*.

Then, substituting the same $f_{GW,sep}^{DL}$ into Eq. (20) and taking f_{ne}=1, the maximum (or critical) separatrix density can be expressed as:

$$n_{e,u}^{crit} = 3.88 \times 10^{14}\ \frac{B^{7/8}\ a^{1/8}\ (P_{SOL}\ l_\parallel^*)^{-1/8}}{{q_c}^{9/8}\ R^{9/8}\ \mu_0} \sqrt{1+k^2}\ F_{AZ}\ . \tag{28}$$

The power flow across the LCFS, P_{SOL}, *is* calculated as:

$$P_{SOL} = P_{OH} + P_{heat} - dW_{dia}/dt - P_{rad}^{bulk} = P_{heat}^{tot} - P_{rad}^{bulk} \tag{29}$$

with P_{OH} being the Ohmic power, P_{heat} the auxiliary heating power either from neutral beam heating (NBI) or from ion cyclotron resonance heating (ICRH), P_{rad}^{bulk} the radiated power from

the bulk plasma, $P_{heat}^{tot} = P_{OH} + P_{heat}$ the total heating power and dW_{dia}/dt the rate of change of the total plasma energy. Under stationary conditions, dW_{dia}/dt=0, we obtain:

$$P_{SOL} = P_{heat}^{tot} - P_{rad}^{bulk} = P_{heat}^{tot}\,(1 - \gamma_{rad}^{bulk}) \tag{30}$$

where γ_{rad}^{bulk} is the radiation fraction from the confined plasma.

We introduce the dimensionless parameter f_{LH} by replacing P_{SOL} in Eq. (30) with $f_{LH}P_{LH}$, where P_{LH} is the threshold power required for the L-H transition;

$$f_{LH} = P_{SOL}/P_{LH}. \tag{31}$$

For the H-mode power threshold we will use the empirical ITPA scaling $P_{LH} = 0.049\,\overline{n_e}^{0.72} B^{0.8} S^{0.94}$ [31], where $\overline{n_e}$ denotes the line-averaged electron density in units of 10^{20} m^{-3} and S is the separatrix surface area. Rewriting this scaling in SI units gives $1.95 \times 10^{-16}\ \overline{n_e}^{0.72} B^{0.8} S^{0.94}$. Since the ITPA scaling was obtained for D plasmas, we are adding the $2/A$ factor, according to the dependence first established in [32]:

$$P_{LH} = \frac{2}{A}\ 1.95\ \times 10^{-16}\ \overline{n_e}^{0.72} B^{0.8} S^{0.94} \tag{32}$$

in order to track the (hydrogen) isotope dependence of the c_Z scaling.

P_{LH} in Eq. (32) must be larger than the power through the separatrix P_{SOL} at the L-H transition, since it is understood to be the total input power into the discharges, and a fraction of this power is radiated in the core (Eq. (32)). The average value of the γ_{rad}^{bulk} parameter in the database used to construct the Martin scaling [31] is not known, except that data points with $\gamma_{rad}^{bulk} > 0.5$ were excluded from the database.

In our analysis of the SOL plasma we are using the separatrix electron density $n_{e,u}$ instead of the line-average density $\overline{n_e}$. To relate the two, we are introducing the dimensionless parameter $f_{sep} = n_{e,u}/\overline{n_e}$. Combining Eqs. (2), (28) and (32) to eliminate $\overline{n_e}$ ($\overline{n_e} = n_{e,u}/f_{sep} = f_{ne} n_{e,u}^{crit}/f_{sep}$) and S and Eq. (30) for P_{SOL}, we arrive at:

$$P_{SOL} = \tag{33}$$

$$4.41\ f_{LH}^{0.92} \left(\frac{f_{ne}}{f_{sep}}\right)^{0.66} \frac{l_{\parallel}^{*\,-0.083}}{q_c^{0.74}}\ B^{1.31}\ R^{1.06}\ (1+k^2)^{0.76}\ \varepsilon^{0.95}\ \frac{F_{AZ}^{0.66}}{A^{0.92}}\,.$$

It should be noted that the f_{sep} parameter may be significantly different in a much larger size fusion reactor than in the present existing machines, e.g., due to the difference in neutral opacity and transport at the edge. Hence, it is an important parameter in the scaling of c_Z required for divertor detachment from the point of view of the implications of such a high c_Z on future fusion reactors.

4.1 Scalings for the tokamak near scrape-off layer H-mode power width

The most commonly used scaling for the power width is a multi-machine scaling for upstream power fall-off length derived by Thomas Eich [18] (see Appendix B). A comparison of this scaling with a heuristic drift-based model [19] (HD model) shows satisfactory agreement in both absolute magnitude and power-law dependencies on plasma parameters achieved in a wide range of experiments in D plasmas. Note that in contrast to the HD model, the Eich scaling has no explicit isotope mass dependence. Therefore in this paper for the derivation of c_Z we will use the power width scaling based on the HD model with an explicit isotope mass dependence. This model predicts the following power width, expressed as a decay length of the power flux λ_q:

$$\lambda_q{}^{HD} =$$

$$5671\ (P_{SOL} l_{\parallel}^{*})^{1/8} \frac{(1+\kappa^2)^{5/8} a^{17/8} B^{1/4}}{{I_p}^{9/8} R} \left(\frac{2\overline{A}}{1+\overline{Z}}\right)^{7/16} \left(\frac{Z_{eff}+4}{5}\right)^{1/8} \tag{34}$$

where dimensional variables are expressed in SI units, Z_{eff} and $\bar{Z}$ are 'effective charge' and 'average charge' of all ions. In the case of only singly charged ions $\bar{Z} = Z_{eff}$. Note that the HD model's result shown in Eq. (34) represents the poloidally averaged value of the power scrape-off width.

Eliminating the plasma current dependence by using Eq. (18) the above equation can be written as:

$$\lambda_q{}^{HD} =$$

$$3.6 \times 10^{-4}\ (P_{SOL} l_{\parallel}^{*})^{1/8}\ {q_c}^{9/8} (R/a)^{1/8} B^{-7/8} \frac{1}{(1+\kappa^2)^{1/2}} \left(\frac{2\overline{A}}{1+\overline{Z}}\right)^{7/16} \left(\frac{Z_{eff}+4}{5}\right)^{1/8} \tag{35}$$

where q_c is the cylindrical approximation for the safety factor.

The most recent publication [33] discusses the applicability of the HD model's expression for λ_q at high collisionality expected in high density plasmas reaching the H-mode density limit. Thomas Eich derives a generalized power width scaling $\lambda_q \propto \rho_p\,(1 + 2.1\alpha_t^{1.7})$ where α_t is the normalized collisionality $\alpha_t = 3 \cdot 10^{-18}\, R q_c^2\, n_{e,sep} Z_{eff} T_{e,sep}^{-2}$. In the limit of low edge densities ($\alpha_t \leq 0.2$) the experimental the data base shows a good agreement of this scaling with the IR based multi-machine power width scaling. At elevated separatrix densities ($\alpha_t \geq 0.2$) the power width is broadened.

4.2 Scaling of impurity fractions by using Heuristic drift-based model for the heat flux width

Inserting λ_q^{HD} (Eq. 35) and P_{SOL} (Eq. 33) into Eq. (27) and using Eqs. (26) with the definition of F_{AZ}, G_A and G_Z parameters, together with the expression for the poloidally averaged poloidal magnetic field

$$B_\theta = \frac{\mu_0 I_p}{2\pi a\sqrt{(1+k^2)/2}} = \frac{B\,\epsilon}{q_c}\sqrt{(1+k^2)/2} \tag{36}$$

we obtain:

$c_Z =$

$$0.76 \times 10^{-39}\ \ \frac{B^{1.47}}{L_{INT}}\ \ R^{1.59}\,\frac{f_{LH}^{1.38}}{f_{ne}\,f_{sep}}\,\frac{q_c^{0.39}(1+k^2)^{0.14}}{l_\parallel^{*\,0.62}}\,\frac{1}{\epsilon^{0.08}}\,\frac{1}{A^{1.38}}\,\frac{1}{G_A^{1.19} G_Z^{0.38}}\,. \tag{37}$$

This scaling, with an explicit isotope mass dependence, will be used to predict the required impurity fractions for divertor detachment for diverse impurity species in future tokamak reactors ITER and DEMO in the following section. The presence of the f_{sep} parameter in the above equation compensates for the appearance of the line-average density $\overline{n_e}$ in the H-mode power threshold scaling Eq. (32) instead of the separatrix density $n_{e,u}$, which is a more relevant parameter for the L-H transition physics.

Potential implications of the model projections to a fusion reactor that may need to operate at a density limited by other physical and technological challenges is discussed in Appendix E.

5. Discussion

By retaining only the main dependences, Eq. (37) can be written as:

$$c_Z \propto \frac{B^{1.47}}{L_{INT}} \; R^{1.59} \frac{q_c^{0.39}(1+k^2)^{0.14}}{\epsilon^{0.08}} \; \frac{1}{A^{1.38}} \; \frac{f_{LH}^{1.38}}{f_{ne}\, f_{sep}} \,. \tag{38}$$

Note that parameter f_{LH} can be below unity, since it gives the ratio of the power flux to the SOL, P_{SOL}, to the H-mode power threshold on the total input power, P_{LH}, which includes core radiation. Parameter $l_{\parallel}^{*}$, figuring in Eq. (37), is not present in the above scaling. It can be considered constant unless one is interested in advanced magnetic configurations with very long divertor legs.

As shown in Appendix C, the last term $\frac{1}{G_A^{1.19} G_Z^{0.38}}$ on the RHS of Eq. (37) doesn't deviate strongly from unity and therefore can be ignored.

Assuming operation above the L-H threshold power at fixed f_{LH} (values of ≈ 1.2 are often quoted in projections for future machines), the scalings Eqs. (37,38) exhibit a strong dependence on toroidal field, B, and the machine size: $c_Z \propto B^{1.47} R^{1.59}$. Note that the c_Z scaling derived by Reinke [15] is different: $c_Z \propto B^{0.88} R^{1.33}$.The main reason for the divergence of our scaling from that of Reinke is our use the scaling expression for $n_{e,u}^{crit}$ instead of $n_{e,u}$ or f_{GW}, which is dependent on both B and R. Nevertheless, both scalings carry the same message of how to solve the heat exhaust problem in the fusion devices. Since the cost-effective approach to the reactor design requires $BR \sim constant$, similarly to [15], the scaling obtained in this work predicts (albeit marginally) that the reactor would benefit more from higher toroidal field than from larger machine size.

Extrapolation from existing medium-size devices such as JET-ILW to a reactor-scale tokamaks such as DEMO (EU DEMO 1 design) ($B = 2.5\,T \rightarrow 5.7\,T;\; R = 2.9\,m \rightarrow 9.1\,m$) implies the need to increase impurity fractions by factor 21, based only on magnetic field and machine size dependencies ($c_Z \propto B^{1.47} R^{1.59}$). This factor however is strongly reduced (down to 7) when an expected increase of the integral L_{INT} (see Eq. (14)) in DEMO is taken into account ($c_Z \propto B^{1.47} R^{1.59}/L_{INT}$): $L_{INT} = 6.63 \times 10^{-30}\; W\, m^3 eV^{3/2} \rightarrow 18.8 \times 10^{-30}\; W\, m^3 eV^{3/2}$ (see Table 1, which will be discussed later) due to $T_{e,u} = 138\; eV\; (JET - ILW)$ →316 eV (DEMO) for f_{LH}=1.2 (for the N_2 seeding). Here, the upstream separatrix temperature, $T_{e,u}$, is calculated by using Eq. (16), and λ_q is evaluated from the Eich scaling [18].

As has already been pointed out in Sec. 3, at the plasma edge the local coronal equilibrium cannot be assumed for the calculation of radiative losses. In H-mode plasmas ELMs regularly expel particles into the SOL leading to frequent reorganization of profiles. Additionally, fast parallel transport in the SOL leads to a significant reduction of the impurity residence time below the time scales for ionisation and recombination. Hence, the local equilibrium cannot be established and one expects impurities to enter the plasma as neutrals and emit line radiation during an early ionisation phase. Usually, the radiative loss function L_Z is enhanced by deviations from coronal equilibrium. The deviation can be described by the product of the electron density and residence time, $n_e\tau$, which in turn is proportional to the ratio of impurity residence (τ) and ionisation times. Large value of this ratio ensures coronal equilibrium. Under non-coronal conditions, radiation increases with decreasing τ.

Fig. 1 shows the cooling rate coefficient L_Z for a number of impurities with several values of the non-coronal parameter $n_e\,\tau$ taken from the ADAS database [34], assuming electron density of 10^{20} m^{-3}, as the sum of line radiation, recombination-induced and bremsstrahlung radiation. In this paper we use polynomial fits applied in [35] which were calculated from ADAS for electron density of 10^{20} m^{-3}, which is a typical value for the divertor SOL. The influence of the residence time of impurities on radiation has been intensively discussed in [36]. ELMs flush out impurities from the pedestal and cause a reorganization of profiles after each ELM crash. The residence time at the pedestal cannot exceed the inverse of the ELM frequency, $1/f_{ELM}$.

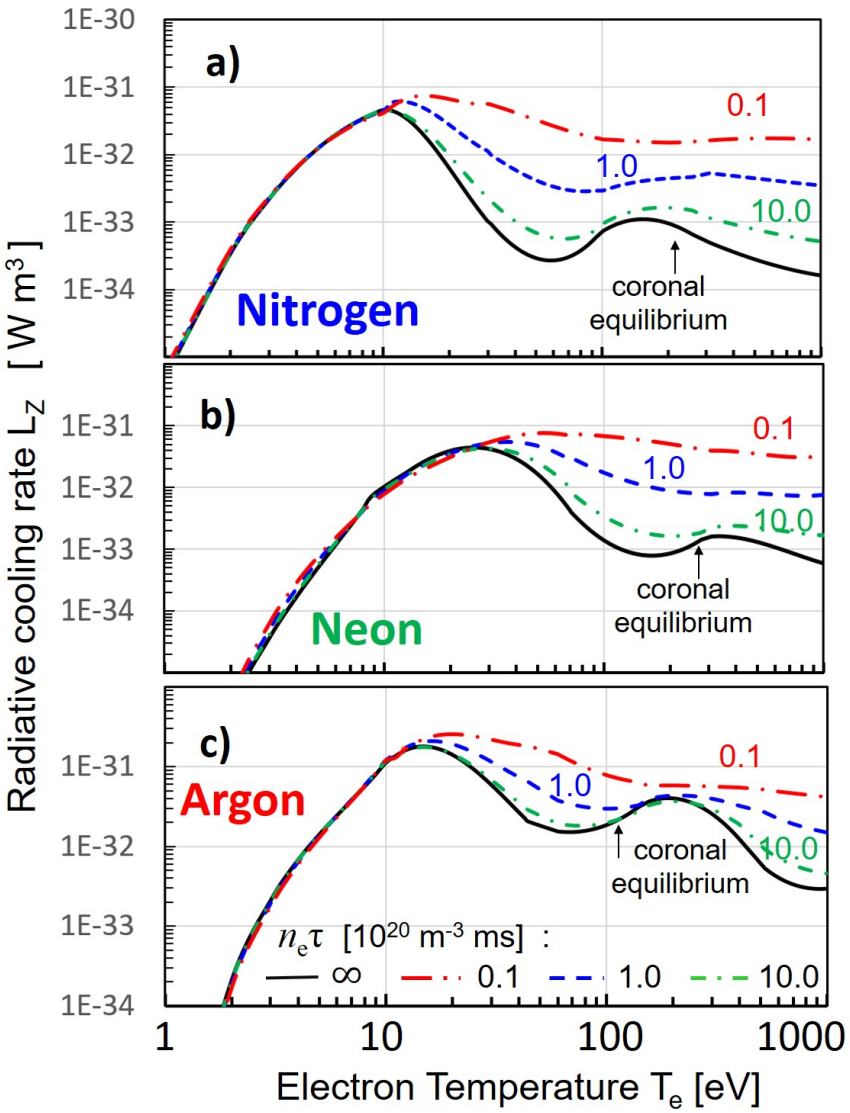

Fig. 1. The cooling rate coefficient L_Z for N_2, Ne and Ar and several assumptions of $n_e\tau$: 0.1×10^{20} m^{-3} ms, 1.0×10^{20} m^{-3} ms and 10.0×10^{20} m^{-3} ms.

Figs. 2 show the function L_{INT} calculated for nitrogen, neon and argon for different assumptions about $n_e\tau$: 1.0×10^{20} and 10.0×10^{20} m^{-3}ms (times are given in milliseconds). These graphs exhibit a strong increase of L_{INT} with the decrease in $n_e\tau$.

Similarly to the paper [14] we compare our empirical scaling with results of Kallenbach's model [13] (see Fig. 4 inside this Ref.), which has been successfully calibrated against AUG

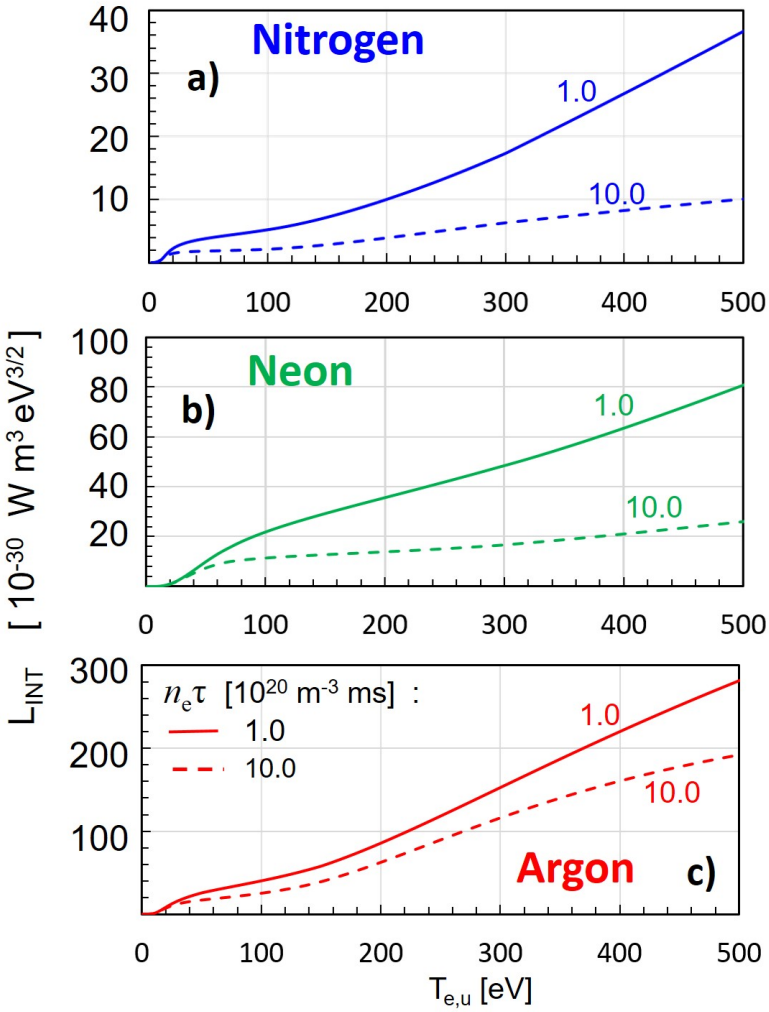

Fig. 2. L_{INT} as a function of $T_{e,u}$ for N_2, Ne and Ar and two values of the non-coronal parameter of $n_e\tau$: 1.0×10^{20} m^{-3} ms and 10.0×10^{20} m^{-3}ms.

experimental data. Plasma parameters discussed in [13] are the following: P_{SOL}=10.8 MW, $n_{e,sep}=7\times10^{19}$ m^{-3}, $L_{||}$=20 m (calculated as $\pi q_{95}R$) and $c_{Z=7}$ =4%. The plasma current of 1.2 MA results in the Greenwald density limit of $n_{GW} = \frac{I_p}{\pi a^2} = 1.44\times10^{20}$ m^{-3}. The density limit achieved in the experiment at I_p=1.2 MA is about 0.85 of the Greenwald density limit and corresponds to the central line-averaged density of about $\bar{n}_e = 1.2\times10^{20}$ m^{-3}. With $\bar{n}_e = 1.2\times10^{20}$ m^{-3} and toroidal field of B=2.5 T we obtain P_{LH}=4.1 MW from Eq. (32) and correspondingly f_{LH}=2.63. Note that such a large f_{LH} factor is not possible in future reactors due to economic cost considerations, where the operation is to take place at f_{LH} factors slightly above 1.0. Using the derived scaling Eq. (38), the reduction of P_{SOL} down to 4.9 MW (corresponding to f_{LH}=1.2),

with all other parameters of the AUG discharge being fixed, will imply the reduced impurity fraction of $c_{Z=7}$=1.6%. Instead of the numerical coefficients in Eq. (37), here we have normalized our empirical scaling to match the experimentally measured value $c_{Z=7}$ = 4%, which was achieved in AUG by approximating the ratio of the D and N valve flows under quasi stationary conditions [13].

In order to estimate impurity fractions required for detachment in existing and future tokamaks, we use AUG, JET-ILW, ITER and DEMO machine engineering parameters listed in Table 2 of Ref. [14]. One of the uncertainties in Eq. (37) is a poorly defined parameter f_{LH}. In Eq. (31) it is defined as a ratio of the total power flux through the separatrix by the H-mode power threshold. It would be natural to assume that f_{LH} has to exceed 1 for the discharge to be in the H-mode. As was pointed out in Sec. 4, owing to non-zero γ_{rad}^{bulk} the degree of excess of f_{LH} over unity cannot be quantified. Here, we will be assuming that it is not large, and, following [14,15] we will be neglecting γ_{rad}^{bulk}. Such an approximation can be justified by a number of simplifications we adopted in our model.

In ITER, P_{SOL}=100 MW is expected in the baseline scanario, and P_{LH} values calculated by Eq. (32) are 89 MW and 71.5 MW at the nominal density of 10^{20}m^{-3} (f_{GW}=0.85) for deuterium and deuterium-tritium (DT) discharges, respectively. Thus, the parameter f_{LH} is 1.12 for the D plasmas and 1.4 for the DT plasmas. On the other hand, in DEMO with an ITER-like divertor configuration, to keep the heat flux density on target below 5−10 MW m^{-2}, up to 70% of the loss power P_{loss} has to be radiated on closed field lines (P_{loss}=P_{heat}+P_{α} ≈450 MW) [37], making it impossible to neglect γ_{rad}^{bulk}. In our calculations we will use $(P_{heat} + P_{\alpha})/P_{LH} \approx 4$. Assuming $\gamma_{rad}^{bulk} = 0.7$ we obtain $f_{LH} \approx 1.2$, when P_{LH} in Eq. (31) is understood to be the critical power for P_{SOL} necessary for the L-H transition. The proper analysis which takes into account the core radiation was done by H. Zohm [38, 39] delivering $f_{LH} = 1.2$ for the DEMO reactor. Therefore, for the cross comparison of these tokamaks we will use factors f_{LH}=1.2 and f_{ne}=0.9.

Taking into account that the electron density of 10^{20} m^{-3} is typical for the divertor SOL in tokamaks with the pronounced detachment, the non-coronal enhancement of the radiation could be approximated by setting the non-coronal parameter $n_e\tau = 1.0 \times 10^{20}\ m^{-3}\ ms$. It should be noted that the residence time τ cannot be specified precisely. However, there are factors that limit the degree of the variation of the product $n_e\tau$. The residence time at the target plate can be lower, below ~ 1 milisecond, due to the back-streaming of the plasma to the target at densities above 10^{20} m^{-3} [13]. At the same time the density decreases towards the outer mid-plane and τ

can increase up to a limit $\tau = 1/f_{ELM}$. Therefore the value of the non-coronal parameter $n_e\tau = 1.0 \times 10^{20}\ m^{-3}\ ms$ is the most likely value and will be used for further study.

Table 1 shows comparisons among recent operating parameters in existing tokamaks and those expected in reactor projects. The estimated nitrogen fraction $c_{Z=7}$ required to prompt the divertor detachment is normalized to the AUG discharge parameters from [13] assuming

	Bt (T)	Ip (MA)	B_θ (T)	a (m)	R (m)	k	q_c	n_{GW} ($10^{20}m^{-3}$)	$T_{e,u}$ (eV)	L_{INT} (10^{-30} Wm^3 $eV^{3/2}$)	$c_{Z=7}$ (%) in D plasmas	$c_{Z=7}$ (%) in D-T plasmas
ASDEX-U	2.5	1.2	0.34	0.52	1.6	1.63	3.16	1.44	115.0	5.7	1.6	1.2*
JET-ILW	2.5	2.5	0.39	0.9	2.9	1.73	2.79	0.98	138.5	6.6	3.4	2.5
ITER	5.3	15	1.03	2.0	6.2	1.8	2.42	1.19	270.0	14.9	14.7	10.8
EU DEMO 1	5.7	20	0.98	2.94	9.1	1.7	2.62	0.74	316	18.8	24.3	17.9

Table 1. Estimated nitrogen fraction $c_{Z=7}$ required for detachment in existing and future tokamaks. Here f_{LH}=1.2, f_{ne}=0.9 and $n_e\tau = 1.0 \times 10^{20}\ m^{-3}\ ms$ are assumed. Calculations are done for pure D and mixed D-T (50%D/50%T) plasmas.

f_{LH}=1.2 and $n_e\tau = 1.0 \times 10^{20}\ m^{-3}\ ms$. The upstream separatrix temperature, $T_{e,u}$, is calculated by using Eq. (16) with $L_\parallel = \pi q_c R$ and λ_q evaluated from the Eich's scaling [18]. Please note that in the expression of $T_{e,u}$ (Eq. 4) it was assumed that the power crossing the SOL flows equally to inner and outer divertors. If some in-out asymmetry occurs, e.g. by 2/3's of P_{SOL} going to the outer divertor (in-out power asymmetry of 1: 2), it will lead to an increase in the upstream electron temperature by 8.6%. In ITER, with P_{SOL}=100 MW, the increase in $T_{e,u}$ by 8.6% (from 270 eV to 293 eV) leads to an increase in L_{INT}. This in turn leads to the c_Z fraction being reduced. In the case of the Ne seeding in ITER, c_Z will be reduced from 4.9% to 4.5%. JET data used in this table are taken from Ref. [40] for the plasma in the ITER-like wall: I_p/B=2.5MA/2.5T, f_{GW}=0.85, q_c=2.79, k=1.73, n_{GW}=9.82×10^{19} m^{-3} and P_{SOL}=11.6 MW at f_{LH}=1.2. The planned ITER operation [41] assumes P_{fus}=500 MW and the fusion energy gain factor Q=10. The EU Demo1 reactor allows core radiation to limit P_{SOL} to the value just above the H-mode power threshold to sustain the H-mode confinement [42].

Table 2 shows, in addition to the nitrogen data, also estimated impurity fractions for Ne and Ar. Calculations for these two gases were done by taking into account corresponding radiative

functions L_{INT}. The usage of neon and argon reduces the impurity fractions in the SOL due to an increase in L_{INT}. Assuming that ITER will operate in the deuterium-tritium (D-T) mixture with 50% of D and 50% of T, the required calculated impurity fractions are 10.1%, 3.4% and 1.0% for N_2, Ne and Ar, respectively. Tables 1 and 2 give c_Z for pure D and mixed D-T

	Nitrogen			Neon			Argon		
	L_{INT} (10^{-30} W m^3 eV$^{3/2}$)	$c_{Z=7}$ (%) in D plasmas	$c_{Z=7}$ (%) in D-T plasmas	L_{INT} (10^{-30} W m^3 eV$^{3/2}$)	$c_{Z=10}$ (%) in D plasmas	$c_{Z=10}$ (%) in D-T plasmas	L_{INT} (10^{-30} W m^3 eV$^{3/2}$)	$c_{Z=18}$ (%) in D plasmas	$c_{Z=18}$ (%) in D-T plasmas
ASDEX-U	5.7	1.6	1.2*	24.2	0.38	0.28*	44.8	0.18	0.13*
JET-ILW	6.6	3.4	2.5	27.6	0.83	0.61	52.9	0.38	0.28
ITER	14.9	14.7	10.8	44.5	4.9	3.6	131.8	1.48	1.1
EU DEMO 1	18.8	24.3	17.9	50.6	9.0	6.6	163.6	2.5	1.8

Table 2. Estimated impurity fractions required for detachment for N_2, Ne and Ar assuming f_{LH}=1.2, f_{ne}=0.9 and $n_e\tau = 1.0 \times 10^{20}\ m^{-3}\ ms$. Calculation are made for pure D and mixed D-T (50%D/50%T) plasmas.

(50%D/50%T) plasmas. The dependence on the isotope mass $c_Z \propto \bar{A}^{-1.38}$ was taken into account in these estimates. It originates from scalings $P_{LH} \propto A^{-1}$, $f_{GW,sep}^{DL} \propto A^{9/16}$ and $\lambda_q{}^{HD} \propto A^{7/16}$.

As shown in Tables 1 and 2, the model predicts a significantly higher c_Z for achieving detachment in a fusion reactor relative to the present experiments. The injection of such a large amount of impurities into the plasma could have two main effects:

• impact on the sputtering yield of tungsten assuming that the target material is made of W and

• impact on the impurity screening by the divertor plasma and thus the transport of impurities into the confined plasma region.

Increased radiative losses lead to lower electron temperatures and thus to much lower sputtering yields. On the other hand, the increased fraction of impurities with a higher net charge and mass causes erosion with higher impact energies and leads to lower sputtering thresholds. Even if sputtering yields of W can be strongly reduced during the inter-ELM phase with advanced detachment at low target T_e, the tungsten sputtering during ELMs will significantly increase the impurity fraction. It should be mentioned that the dominant W erosion mechanism in the divertor is the intra-ELM sputtering induced by impurities as well as hydrogenic ions with energies determined by the pedestal temperature. According to the free streaming model [43], during ELMs electrons, on their way to the divertor target, transfer their parallel energy to ions to maintain quasi-neutrality. It is experimentally observed in type I H-mode discharges that the maximum sum of the ion and electron energy linearly depends on the pedestal electron temperature: $\max(E_i+E_e) = 5.23\times T_{e,ped}$ [44]. The model assumes that only $E_{e,\perp}$ is left in E_e, resulting in almost mono-energetic ions with $E_{i,max}$ up to $4.23\times T_{e,ped}$. Assuming the average incident energy of ions, $\langle E_i \rangle$, of 1keV, the sputtering yield (number of atoms removed from the target surface per incident ion) for Ne is factor 40 larger than for T ions [45]. Accordingly, the fluence of sputtered tungsten per ELM (atoms / ELM) due to neon is at least 1.4 and 2.6 times larger than due to T ions for $c_Z = 3.6\%$ (ITER) and $c_Z = 6, 6\%$ (DEMO) respectively.

Additionally, the injection of large amounts of impurities into the plasma could have strong impact on the impurity screening by the divertor plasma. The screening is determined by the diffusion and convection of impurity ions in the SOL which competes with parallel ion flow towards the divertor targets. The latter is determined by the balance between the thermal force, F_{therm}, and the friction force, F_{fric}, along magnetic field lines [28]. The thermal force, induced by the ion temperature gradient, pushes impurity ions towards higher temperatures, that is, to the main plasma (core-SOL plasma boundary). On the other hand, the frictional force, caused by the plasma flow from the main plasma to the divertor plates, pushes impurity ions to the divertor area. The large fraction of injected impurities could strongly impact the balance between the thermal force, F_{therm}, and the friction force, F_{fric}, along magnetic field lines due to the increased ion temperature gradient. The increased thermal force could push the impurity ions up the temperature gradients, $dT_{e,i}/dl$ to the main plasma (core-SOL plasma boundary) and to the confined plasma region, thereby reducing the impurity screening. This could lead to an increase of the radiative power losses within the confined plasma and consequently could affect the plasma confinement and the fuel dilution.

It should be noted that the power width length λ_q can be widened [33] in the case of high collisionality expected in high density plasmas. As shown in Appendix D, the broader λ_q could lead to a strong reduction of the c_Z required to drive the divertor into the detachment. More investigation of the broadening of λ_q at high collisionality is required.

6. Summary

The goal of this work is to contribute to theoretical understanding of scaling laws for the power exhaust in the plasma boundary necessary to achieve divertor detachment in terms of impurity fractions, for projections onto future machines such as ITER and DEMO. In order to estimate the required impurity fractions a new quantitative scaling law for c_Z in high density H-mode operation close to the density limit was derived. It is based on a simple SOL radiation model and uses dimensionless parameters normalized by empirical scalings for the heat flux width in the SOL, H-mode power threshold, and separatrix density limit caused by an MHD instability. The derived c_z scaling shows strong dependencies on toroidal field, major radius, power to the SOL normalized to the H-mode power threshold, f_{LH}, and to the radiative parameter L_{INT}: $c_Z \propto \frac{B^{1.47}}{L_{INT}} \; R^{1.59} \frac{q_c^{0.39}(1+k^2)^{0.14}}{\epsilon^{0.08}} \; \frac{1}{A^{1.38}} \; \frac{f_{LH}^{1.38}}{f_{ne}\, f_{sep}}$. The scaling also predicts a strong dependence on the average atomic mass $\bar{A}$ of plasma species, $c_Z \propto \bar{A}^{-1.38}$. This strong dependence on the isotopic mass mixture is significant, with c_Z being up to 27% lower in deuterium-tritium (D-T) mixtures using 50% of D and 50% of T, and being 43% lower in the 100% tritium plasmas compared to pure deuterium plasmas. The strong dependence on the isotope mass is attributed mostly to lower H-mode power threshold for larger isotope mass ($P_{LH} \propto A^{-1}$) .

The formulation of the impurity fraction in this paper can be used as a guideline for the machine design and for planning of operational scenarios.

Acknowledgements

This work has been carried out within the framework of the EUROfusion Consortium and has received funding from the Euratom research and training programme 2014-2018 and 2019-2020

under grant agreement No 633053. The views and opinions expressed herein do not necessarily reflect those of the European Commission.

Appendix A

Goldston's model for the density limit [21] is based on the heuristic drift-based model for the power scrape-off width assuming that the H-mode density limit is caused by an MHD instability in the near SOL [21]. An expression for the ballooning parameter α was derived under the assumption that the pressure gradient scale length at the separatrix is approximately equal to λ_q:

$$\alpha \equiv -\frac{Rq^2\beta}{\lambda_q} = \frac{e\,Rq_c{}^2 2n_{e,u}T_e}{\lambda_q B_t^2/2\mu_0} = 4\mu_0 e\,\frac{Rq_c{}^2 n_{e,u}T_e}{\lambda_q B_t^2}\,. \tag{39}$$

Combining Eqs. (16) and (4) to eliminate $q_{\parallel,u}$ and applying $L_\parallel = l_\parallel^*\,\pi q_c R$ we arrive at:

$$T_{e,u} \approx \left(\frac{7\,q_{\parallel,u}\,L_\parallel}{2k_{0,e}}\right)^{\frac{2}{7}} = \left(P_{SOL}\,{}^{B}\!/_{B_\theta}\;\frac{q_c l_\parallel^*}{\left(\frac{2}{7}\right)k_{0,e}\,4\lambda_q}\right)^{\frac{2}{7}}. \tag{40}$$

Substituting B_θ (Eq. 36) and $k_{0,e}$ (Eq. 9) into this equation gives:

$$T_{e,u} \approx \left(\frac{2^{\frac{1}{2}}}{({}^{8}\!/_{7})k_0}\right)^{\frac{2}{7}}\left(\frac{P_{SOL}\,q_c{}^2 l_\parallel^*}{G_Z\epsilon\,\sqrt{1+k^2}\,\lambda_q}\right)^{\frac{2}{7}} = 0.12\,\left(\frac{P_{SOL}\,q_c{}^2 l_\parallel^*}{G_Z\epsilon\,\sqrt{1+k^2}\,\lambda_q}\right)^{\frac{2}{7}}. \tag{41}$$

Introducing the above expression for $T_{e,u}$ into Eq. (39) gives:

$$\alpha = 9.68\times10^{-26}\,P_{SOL}^{2/7}\lambda_q^{-9/7}q_c^{18/7}R^{9/7}a^{-2/7}n_{e,u}B^{-2}(1+k^2)^{-1/7}G_Z^{-2/7}l_\parallel^{*2/7}\,. \tag{42}$$

Assuming $\alpha = \alpha_{crit} \approx C_\alpha(1+\kappa^2)^\gamma$, at which the upstream separatrix density reaches the maximum (critical) density, $n_{e,u} = n_{e,u}{}^{crit}$, Eq. (42) reads:

$$C_\alpha(1+\kappa^2)^\gamma = 9.68\times10^{-26}\,P_{SOL}^{2/7}\lambda_q^{-9/7}q_c^{18/7}R^{9/7}a^{-2/7}n_{e,u}^{crit}B^{-2}(1+k^2)^{-1/7}G_Z^{-2/7}l_\parallel^{*2/7}. \tag{43}$$

Using the expression for λ_q (Eq. 35) which has an $l_\parallel^*$ dependence and $n_{e,u}^{crit} = n_{e,u}|_{(f_{ne}=1)}$ (Eq. 20), the Goldston's equation can finally be obtained:

$$f_{GW,sep}^{DL} = 4.85\,C_\alpha\left(\frac{q_c RB}{a}P_{SOL}l_\parallel^*\right)^{-1/8}(1+\kappa^2)^{\gamma-3/2}\left[\frac{2\bar{A}}{(1+\bar{Z})}\right]^{9/16}\left(\frac{Z_{eff}+4}{5}\right)^{-1/8}. \tag{44}$$

This density limit scaling has the dependence on the dimensionless factor l^* which takes into the account a possibility of extended field lines in alternative configurations.

Appendix B

The most commonly used scaling for the upstream power fall-off length in the SOL is a multi-machine scaling obtained for the OMP position [18]:

$$\lambda_{q,mp} = 0.73\, B^{-0.78} {q_c}^{1.2} {P_{SOL}}^{0.1}\, R^{0.0} \tag{45}$$

where λ_q is in units of mm, mapped to the OMP position, and P_{SOL} is in MW. This empirical scaling is based on extensive infrared thermography measurements of the power decay length in the SOL on several machines including JET and AUG [18]. Here we also present it in SI units:

$$\lambda_{q,mp} = 1.83\ \times 10^{-4}\, B^{-0.78} {q_c}^{1.2} {P_{SOL}}^{0.1}\, R^{0.0}\ . \tag{46}$$

At the same time, the power decay length in the SOL λ_q used in Eq. (27) is the poloidally averaged quantity. As it is shown in [18], the two decay lengths are connected by:

$$\lambda_{q,mp} = \frac{R}{(R+a)} \quad \frac{B_\theta}{B_{\theta,mp}}\, \lambda_q \tag{47}$$

where $B_{\theta,mp}$ is the poloidal magnetic field at the outer midplane and

$$B_\theta = \frac{\mu_0 I_p}{2\pi a\sqrt{(1+k^2)/2}} = \frac{B\,\epsilon}{q_c}\sqrt{(1+k^2)/2} \tag{48}$$

is the poloidal field poloidally averaged around the plasma. Numerically, as it is found in [18], on average $\lambda_{q,mp} = (0.55 \pm 0.05)\ \times \lambda_q$ for all data points used in [18]. For comparison of experimental and theoretical power width, it is required to map ${\lambda_q}^{HD}$ to the outer midplane.

For further usage of this experimental scaling for the comparison with theoretically predicted power width (HD), we rewrite Eq. (46) via the poloidally averaged λ_q:

$$\lambda_q = \lambda_{q,mp}/0.55 = 3.33\ \times 10^{-4}\, B^{-0.78} {q_c}^{1.2} {P_{SOL}}^{0.1}\, R^{0.0}\ . \tag{49}$$

A comparison of this scaling with a heuristic drift-based model [19] (HD model) shows a satisfactory agreement in both absolute magnitude and power-law dependencies on plasma parameters achieved in a wide range of experiments.

Appendix C

In this section we review expressions for $\frac{1}{G_A^{1.19} G_Z^{0.38}}$, the final term on the RHS of Eq. (37), where

$$G_A = \frac{\bar{A}}{1+\bar{Z}} \text{ and } G_Z = \frac{5}{Z_{eff}+4}$$

$$\bar{A} = \sum_i n_i A_i / \sum_i n_i, \qquad \bar{Z} = n_e / \sum_i n_i, \quad Z_{eff} = \frac{\sum n_i {Z_i}^2}{n_e} . \tag{50}$$

Assuming the plasma with the mix of hydrogen isotopes with the average atomic mass A_H and a single dominant impurity we find:

$$1 + \bar{Z} = 1 + \frac{n_e}{n_H + n_Z} \tag{51}$$

$$\bar{A} = \frac{n_H A_H + n_Z A_Z}{n_H + n_Z} \tag{52}$$

$$Z_{eff} = \frac{n_H}{n_e} + \frac{n_Z Z^2}{n_e} . \tag{53}$$

We can express n_H via c_Z and n_e, using the plasma ambipolarity condition: $n_e = n_H + Z n_Z = n_H + Z c_Z n_e$. Here we used the definition of the $c_Z = n_Z / n_e$.

Hence

$$n_H = n_e - Z c_Z n_e = n_e (1 - c_Z Z) . \tag{54}$$

Inserting n_H into Eqs. (51-53) gives new expressions for $1 + \bar{Z}$, $\bar{A}$ and Z_{eff} :

$$1 + \bar{Z} = \frac{2 - c_Z (Z-1)}{1 - c_Z (Z-1)} \tag{55}$$

$$\bar{A} = \frac{A_H (1 - c_Z Z) + A_Z c_Z}{1 - c_Z (Z-1)} \tag{56}$$

$$Z_{eff} = 1 + c_Z (Z^2 - Z) . \tag{57}$$

From these equations it follows that:

$$G_A = \frac{\bar{A}}{1+\bar{Z}} = \frac{A_H (1 - c_Z Z) + A_Z c_Z}{2 - c_Z (Z-1)} . \tag{58}$$

$$G_Z = \frac{5}{Z_{eff}+4} = \frac{5}{5+c_Z\,(Z^2-Z)}\,. \tag{59}$$

Combining these results in a new expression for $\frac{1}{G_A^{1.19}G_Z^{0.38}}$, which is the final term on the RHS of Eq. (37), gives:

$$\frac{1}{G_A^{1.19}G_Z^{0.38}} = \left[\frac{2-c_Z(Z-1)}{A_H(1-c_ZZ)+A_Zc_Z}\right]^{1.19}\left[\frac{5}{5+c_Z\,(Z^2-Z)}\right]^{-0.38}\,. \tag{60}$$

Fig. 3 shows the dependence of this term on the impurity fraction c_Z in pure deuterium (A_H=2)

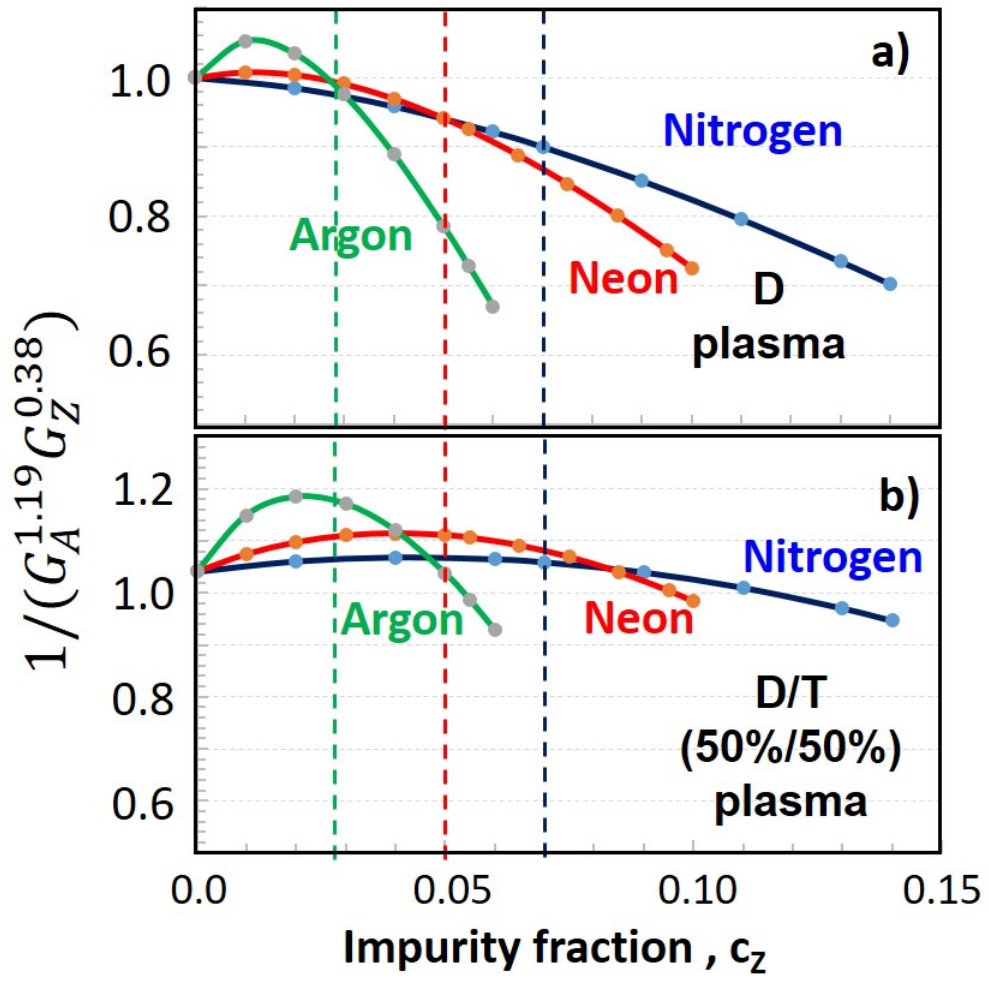

Fig. 3 Dependence of the function $1/(G_A^{1.19}G_Z^{0.38})$ on impurity fraction c_Z.

and mixed (50%/50%) deuterium-tritium plasmas (A_H=2.5). The calculation is done for

different impurities with Z=7, 10 and 18 (nitrogen, neon and argon) and corresponding to impurity masses A_Z=14, 20 and 40, respectively.

Dashed lines represent c_Z fractions for each species (Z) at which 50% of deuterons are replaced with impurity ions, c_Z^*. For $c_Z \leq c_Z^*$ deviations from unity are very moderate:

- D plasmas: maximum 10% and 6% reduction in c_7 and c_{10}, respectively, and 5% increase in c_{18}.
- D-T plasmas: maximum 7%, 11% and 18% increases in c_7, c_{10}, and c_{18}, respectively.

Due to smallness of these variation we will neglect this term in Eq. (37).

Appendix D

The normalized collisionality α_t could have an impact on the c_Z scaling. Here we will extract the dependence of the most important parameters such as P_{SOL}, $f_{GW,sep}^{DL}$ and $n_{e,sep}^{crit}$ on the collisionality α_t.

As already shown in section 4.1, $\lambda_q \propto (1 + 2.1\alpha_t^{1.7})$ in the experiment. The following dependencies could be derived from λ_q and Eq. (43):

$$n_{e,sep}^{crit} \propto (1 + 2.1\alpha_t^{1.7})^{\frac{9}{7}} \times P_{SOL}^{-1/8} \quad (61)$$

$$f_{GW,sep}^{DL} \propto (1 + 2.1\alpha_t^{1.7})^{9/7} \times P_{SOL}^{-1/8} \quad (62)$$

By using Eqs. (31,32) and $\overline{n_e} \propto n_{e,u}^{crit}$ one obtains

$$P_{SOL} \propto (1 + 2.1\alpha_t^{1.7})^{0.85} \quad (63)$$

Eqs. (61) and (62) could be rewritten as:

$$n_{e,sep}^{crit} \propto (1 + 2.1\alpha_t^{1.7})^{1.18} \quad (64)$$

$$f_{GW,sep}^{DL} \propto (1 + 2.1\alpha_t^{1.7})^{1.18} \quad (65)$$

Finally, from Eq. (22) one obtains the following dependence of c_Z on the normalized collisionality α_t

$$c_Z \propto (1 + 2.1\alpha_t^{1.7})^{-2.725} \quad (66)$$

The α_t above is the normalized collisionality $\alpha_t = 3 \cdot 10^{-18}\, R q_c^2\, n_{e,sep} Z_{eff} T_{e,sep}^{-2}$, where R and $n_{e,sep}$ are given in SI units, m and m^{-3} and T_e in eV.

For the c_Z=c_Z^* fractions for each species (Z) at which 50% of deuterons are replaced with impurity ions, the Z_{eff} values , calculated from Eq. (51), are 3.98, 5.5 and 9.5 for N_2, Ne and Ar

seeded species respectively. Such Z_{eff} values could lead to a strong reduction of the $(1+2.1\alpha_t^{1.7})^{-2.725}$ factors. For example these factors in the Neon seeded case are $(1+2.1\alpha_t^{1.7})^{-2.725}$=0.48 and $(1+2.1\alpha_t^{1.7})^{-2.725}$=0.60 for ITER and DEMO plasmas, respectively, indicating the strong reduction of c_Z to achieve the pronounced detachment.

Appendix E

In this section we discuss potential implications for our model projections to a fusion reactor which have to be operated at densities limited by other physical and technological challenges. These can be included by deriving the c_Z scalinlg vs. $n_{e,u}$ or $f_{GW,sep}$.

We will use Eq. (22) and replace λ_q with the expression ${\lambda_q}^{HD}$ (Eq. 35):

$$c_Z = 1.11\times10^{-39}\, P_{SOL}^{5/4}\, \frac{B^{19/28}}{B_\theta^{10/7}}\, \frac{\epsilon^{5/28}\,(1+k^2)^{-9/7}}{{f_{GW,sep}}^2\; q_c^{5/28}\quad L_{INT}\, l_\parallel^{*3/4}}\, \frac{G_Z^{-1/4}}{G_A^{5/8}} \tag{67}$$

Combining Eqs. (19), (31) and (32) we arrive at:

$$P_{SOL} = 1.9\;\; \frac{f_{LH}}{A}\left(\frac{f_{GW,sep}}{f_{sep}}\right)^{0.72} B^{1.52}\, R^{1.16}\, \frac{\left(1+k^2\right)^{1.19}\varepsilon^{0.94}}{q_c^{0.72}} \tag{68}$$

Inserting the above expression for P_{SOL} into Eq. (67) gives:

$$c_Z = 4.06\times10^{-39}\, \frac{{f_{LH}}^{5/4}}{A^{5/4}}\, \frac{B^{1.15}R^{1.45}}{{f_{GW,sep}}^{1.1}{f_{sep}}^{0.9}}\;\; \frac{q_c^{0.35}}{\epsilon^{0.075}(1+k^2)^{0.51}\, l_\parallel^{*3/4}}\;\; \frac{1}{L_{INT}}\, \frac{G_Z^{-1/4}}{G_A^{5/8}} \tag{69}$$

Similar results for the c_Z scaling were obtained in the previous study in [15] (Eqs. (10)). It should be noted that the scaling for c_Z in [15] shows the f_{GW} dependence and, for comparison with Eq. (69), f_{GW} should be replaced by $f_{GW} = f_{GW,sep}\, f_{sep}$. Small differences in the c_Z scalings can be explained by Matt Reinke's using the multimachine scaling for the upstream heat flux width $\lambda_q = 1.35\times {P_{SOL}}^{-0.02}\; R^{0.04}\, {B_\theta}^{-0.92}\epsilon^{0.42}$ instead of ${\lambda_q}^{HD}$. In contrast to the heuristic drift based model power width scaling (${\lambda_q}^{HD} \propto {P_{SOL}}^{\frac{1}{8}}$, $Eq.35$) as well as to the Eich scaling ($\lambda_q \propto {P_{SOL}}^{0.1}$, $Eq.45$), this scaling has practically no P_{SOL} dependence. The main advantages of the scaling in Eq. (69) is the presence of the isotope mass dependence which originates from the scalings $P_{LH} \propto A^{-1}$ and ${\lambda_q}^{HD} \propto A^{7/16}$.

References

[1] M Shimada et al. Progress in the ITER Physics Basis Chapter 1: Overview and summary 2007 Nucl. Fusion 47 S1

[2] Zohm H. *et al* 2013 *Nucl. Fusion* **53** 073019

[3]Kallenbach A. *et al* 2015 *Nucl. Fusion* **55** 053026

[4] Bernert M *et al* 2017 *Nucl. Mater. Energy* 1**2** 111–8

[5] Goetz J. *et al* 1996 *Phys. Plasmas* **3** 1908

[6] Reinke M.L. *et al* 2019 *Nucl. Fusion* **59** 046018

[7] Wischmeier M. *et al* 2015 J. *Nucl. Mater.* **463** 22–9

[8] Huber A. *et al* 2020 *Phys. Scr.* **T171** 014055 (7pp)

[9] A Loarte et al. Progress in the ITER Physics Basis Chapter 4: Power and particle control 2007 Nucl. Fusion 47 S203

[10] Raffray A. R. *et al* 2010 *Fusion Eng. Des*. **85** 93–108

[11] Bonnin X. et al 2017 *Nuclear Materials and Energy* **12** 1100–1105

[12] Post D. *et al* 1995 *Phys. Plasmas* **2** 2328

[13] Kallenbach A. *et al* 2016 *Plasma Phys. Control. Fusion* **58** 045013

[14] Goldston R. J. *et al* 2017 *Plasma Phys. Control. Fusion* **59** 055015

[15] Reinke M. L. *et al* 2017 *Nucl. Fusion* **57** 034004

[16] Pitcher C S and Stangeby P C 1997 Plasma Phys. Control. Fusion 39 779

[17] Huber A et al., 2020 Phys. Scr. 2020 014055

[18] Eich T. *al* 2011 *Phys. Rev. Lett.* **107** 215001

[19] Goldston R. J. 2012 *Nuclear Fusion* **52** 013009

[20] Shimomura Y. et al. 2001 *Nucl. Fusion* **41** 309

[21] Goldston R.J. *et al* 2015 *J. Nucl. Mater.* **463** 397–400

[22] Huber A. *et al* 2017 *Nucl. Fusion* **57** 086007

[23] Ghendrih P. *et al* 2007 *J. Nucl. Mater.* **363–365** 581–5

[24] Spitzer L. and Härm R. 1953 *Phys. Rev*. **89** 977

[25] Braginskii S. I. 1965 *Rev. Plasma Phys*. **1** 205

[26] Huber A. and Chankin A. V. 2017 *Plasma Phys. Control. Fusion* **59** 064007 (6pp)

[27] Lengyel L L 1981 IPP Report 1/191

[28] Stangeby P. C. 2000 *The Plasma Boundary of Magnetic Fusion Devices,* Institute of Physics Publishing, Bristol, UK

[29] Bateman G. *et al* 2003 *Phys. Plasmas* **10** 4358

[30] Tokar M. *et al Physics of Plasmas* **16**, 020704 (2009)

[31] Martin Y.R. *et al* 2008 *J. Phys.: Conf. Ser.* **123** 012033

[32] Righi E. *et al* 1999 *Nucl. Fusion* **39** 309

[33] T. Eich et al 2020 Nucl. Fusion 60 056016

[34] ADAS, www.adas.ac.uk/manual.php

[35] Mavrin A. A. 2017 *Journal of Fusion Energy* **36** 161

[36] Casali L. *et al* 2018 *Phys. Plasmas* **25** 032506

[37] Wischmeier M *et al* 2015 *J. Nucl. Mater.* **463** 22

[38] Zohm H. 2019 *Phil. Trans. R. Soc.* A **377**: 20170437. (http://dx.doi.org/10.1098/rsta.2017.0437)

[39] Zohm, H. 2019. *J Fusion Energy* **38,** 3–10 (https://doi.org/10.1007/s10894-018-0177-y)

[40] Giroud C. *et al* 2015 *Plasma Phys. Control. Fusion* **57** 035004

[41] Kukushkin A. S. *et al* 2013 *J. Nucl. Mater.* **438** S203

[42] Wenninger R. *et al* 2015 *42nd EPS Conf. on Controlled Fusion and Plasma Physics (Lisbon, Portugal)* (http://ocs.ciemat.es/EPS2015PAP/pdf/P4.110.pdf)

[43] Moulton D. *et al* 2013 Plasma Phys. and Control. Fus. **55** 085003

[44] Guillemaut Ch. *et al* 2018 Nucl. Fusion **58** 066006

[45] Brezinsek S. *et al* 2019 Nucl. Fusion **59** 096035